Structure of Interannual-to-Decadal Climate Variability in the Tropical Atlantic Sector

ALFREDO RUIZ-BARRADAS, JAMES A. CARTON, AND SUMANT NIGAM

Department of Meteorology, University of Maryland at College Park, College Park, Maryland

(Manuscript received 21 July 1999, in final form 3 December 1999)

ABSTRACT

A search for coupled modes of atmosphere–ocean interaction in the tropical Atlantic sector is presented. Previous studies have provided conflicting indications of the existence of coupled modes in this region. The subject is revisited through a rotated principal component analysis performed on datasets spanning the 36-yr period 1958–93. The analysis includes four variables, sea surface temperature, oceanic heat content, wind stress, and atmospheric diabatic heating. The authors find that the first rotated principal component is associated with fluctuations in the subtropical wind system and correlates with the North Atlantic oscillation (NAO), while the second and third modes, which are the focus of interest, are related to tropical variability.

The second mode is the Atlantic Niño mode with anomalous sea surface temperature and anomalous heat content in the eastern equatorial basin. Wind stress weakens to the west of anomalously warm water, while convection is shifted south and eastward. Surface and upper-level wind anomalies of this mode resemble those of El Niño–Southern Oscillation (ENSO) events. When the analysis is limited to boreal summer, the season of maximum amplitude, the Atlantic Niño mode explains 7.5% of the variance of the five variables. Thermodynamic air–sea interactions do not seem to play a role for this mode.

The third mode is associated with an interhemispheric gradient of anomalous sea surface temperature and a dipole pattern of atmospheric heating. In its positive phase anomalous heating occurs over the warmer Northern Hemisphere with divergence aloft shifting convection to the north and west of the equator and intensifying the subtropical jet stream, while descending motion occurs on the western side of the Southern Hemisphere. Surface and subsurface structures in the ocean are controlled by surface winds. This interhemispheric mode is strongest in boreal spring when it explains 9.1% of the combined variance of the five variables. Thermodynamic air–sea interactions do seem to control the associated sea surface temperature anomalies, although equatorial dynamics may play a role as well.

The authors also examine the connection of the tropical Atlantic to other basins. ENSO events cause patterns of winds, heating, and sea surface temperatures resembling the interhemispheric mode described above. The lag between changes in the Atlantic and Pacific is 4–5 months for the interhemispheric mode. In contrast, no significant impact of ENSO is found on the Atlantic Niño mode. Likewise, no impact of the midlatitude North Atlantic (the NAO) is found on the Tropics, but some impact of the Tropics is found on the midlatitude North Atlantic.

1. Introduction

Early observational studies of the causes of tropical rainfall fluctuations in the Atlantic sector focused attention on the connection to anomalies of sea surface temperature (SST) (Merle 1980; Hisard 1980; Moura and Shukla 1981). These studies found two different SST patterns. The first was a northward shift of tropical convection in the western Atlantic in response to an anomalous northward gradient of SST in boreal spring, an interhemispheric mode often referred to as the Atlantic dipole. The second was a southward shift of convection in the eastern Atlantic in response to rising SST in boreal summer, a phenomenon we refer to as the Atlantic Niño. The existence of the first mode was confirmed apparently by studies examining the principal components of SST variability (Weare 1977; Servain 1991; Nobre and Shukla 1996; Chang et al. 1997) and has also been supported by examination of the dynamical processes by which SST influences meteorology (Hastenrath and Greischar 1993) and by which meteorology influences SST (Carton et al. 1996; Delworth and Mehta 1998). However, it was pointed out by Houghton and Tourre (1992) and Enfield and Mayer (1997) that the requirement of orthogonality of spatial patterns imposes an unnecessary constraint on the analysis. They found that if that constraint was dropped then SST anomaly patterns in the Northern and Southern Hemispheres tend to act independently.

Recently, a number of studies have appeared examining decadal tropical and midlatitude Atlantic climate variability. Some of these studies (Rajagopalan et al. 1998; Robertson et al. 1998; Tourre et al. 1999) suggest

Corresponding author address: Dr. James A. Carton, Department of Meteorology, University of Maryland at College Park, College Park, MD 20742-2425.
E-mail: carton@atmos.umd.edu

that tropical ocean–atmosphere interaction variability can perturb the North Atlantic. This Tropics–midlatitude connection is mostly identified through inspection of spatial patterns from modeling experiments (Robertson et al. 2000) and empirical analyses (Tourre et al. 1999; Rajagopalan et al. 1998). In both cases, however, correlations do not reach high values. However, Robertson et al. (2000) suggest that sea surface temperature anomalies in the tropical and subtropical South Atlantic (rather than those in the northern tropical Atlantic) affect the North Atlantic variability. Mehta (1998) suggests a relation between tropical and extratropical annual SST anomalies, but concludes that ''there was no dynamical–thermodynamical, dipole mode of SST variations.'' Instead the author argues for SST anomalies occurring independently in each hemisphere. Finally, Xie and Tanimoto (1998) and Tanimoto and Xie (1999) propose through modeling and empirical studies that decadal extratropical forcing of the Tropics, excited by the North Atlantic oscillation (NAO), can force a dipole pattern linking the two hemispheres.

In addition to the tropical–midlatitude link, there is also evidence of a tropical connection between El Niño events in the Pacific and anomalously warm events in the northern tropical Atlantic. Lanzante (1996) and Enfield and Mayer (1997) show correlations of 0.5 between those areas and events with a 4–5-month lag. Enfield and Mayer (1997) state that 25% of the variance of the interhemispheric mode is forced by El Niño–Southern Oscillation (ENSO) events. A relationship between the Atlantic Niño mode and Pacific variability has also been suggested by previous studies (Servain 1991; Carton and Huang 1994). They suggest a relaxation of the trade winds in the western Atlantic leads to an accumulation of warm water. Servain (1991) shows a mean correlation of -0.28 when the southern Atlantic (south of 5°N) leads ENSO events (cool events) by 6–11 months; Enfield and Mayer (1997) show a correlation of -0.3 with the principal component time series of their southern Atlantic mode when this lags ENSO events by 4 months, while Zebiak (1993) with his equatorial Atlantic index (3°S–3°N) found a -0.07 correlation. We reexamine these relations here in order to determine what fraction of the variance associated with our Atlantic modes could be forced remotely.

In spite of all the research cited above, there is still disagreement over the identification of coherent modes of variability in the atmosphere and ocean in the tropical Atlantic and their structure. We believe that part of the disagreement results from attempts to identify these modes based solely on ocean data. Here we revisit the issue of coupled modes in the tropical Atlantic sector. Since modes of the coupled system must involve both atmospheric and oceanic variables, we undertake a combined analysis of variables in both fluids. The variables we consider include surface variables (SST, surface wind stress), a measure of ocean dynamical processes (ocean heat content), and a measure of atmospheric convection (diabatic heating). Two of these variables have only recently become available as the result of reanalysis projects. Our approach is to compute the leading structures of recurrent variability from the covariance matrix of the combined normalized variables using the singular value decomposition (SVD) method to compute eigenvectors and eigenvalues efficiently. Then an orthogonal rotation is applied to the extracted eigenvectors. The percentages of explained variance decrease rapidly as atmospheric and oceanic variables are added since only those motions involving both fluids (and properly represented in the datasets) are identified. Thus the reader should expect the principal modes to explain small fractions of the total variance.

In addition to identifying and characterizing coupled modes of variability and their seasonality we would like to understand their relationship to other variables and to remote influences. To explore these relationships we present a series of studies of the strength of the regression of other variables upon the component time series of the modes as well as against indices associated with other phenomena on the tropical Atlantic. In this way we explore the covariations of a variety of variables not part of the original analysis.

2. Data and method

Observation data used in this study are monthly sea surface temperature, 0–276-m ocean heat content, wind stress, residually diagnosed atmospheric diabatic heating at 500 mb and horizontal divergence at 850 and 200 mb. Sea surface temperature and winds are obtained from the Comprehensive Ocean–Atmosphere Data Set analysis of da Silva et al. (1994), which is available for the period 1950–93. Subsurface temperatures are available from the ocean data assimilation analysis of Carton et al. (2000a,b) and Chepurin and Carton (1999) for the period 1950–96. The analysis uses nearly all historical temperature and salinity measurements as constraints on the upper levels of an ocean general circulation model. Heat content has been computed by integration of ocean temperature from the surface to 276-m depth. This depth has been chosen based on results of D. Blankinship (1997, personal communication) who found that at a depth of 240 m 95% of the temperature variability is captured.

In the Tropics atmospheric circulation is driven to a significant degree by the distribution of diabatic heating and associated convergences near the surface and divergences aloft. We examine the relationship of these fields to oceanic variables by including diabatic heating in the combined variability analysis. The diabatic heating is residually diagnosed (e.g., Nigam 1994; Nigam et al. 2000) from the National Centers for Environmental Prediction (NCEP) reanalysis for the period 1958–93. The pressure level of diabatic heating included in our analysis, 500 mb, has been chosen to be consistent with its climatological maximum (the results are insensitive

to this choice). The levels of divergence/convergence, 850 and 200 mb, have been chosen to define the circulation above and below the height of maximum heating. A secondary analysis was carried out using the European Centre for Medium-Range Weather Forecasts (ECMWF) reanalysis. The results were consistent with those produced using the NCEP reanalysis, but the period of the ECMWF dataset is shorter (1979–93).

Some of the datasets such as surface winds and SST have long-term trends. In the case of surface winds these trends are likely to be spurious, possibly associated with changes in measurement platforms (Clarke and Lebedev 1997). In order to minimize the effect of these trends on the analysis we have removed a linear trend from all datasets at each spatial location using a least squares technique. Following this detrending monthly anomalies are calculated with respect to the seasonal cycle computed from their respective record for the common 36-yr period of 1958–93; our primary dataset was thus formed. This record may be too short for detection of asynchronous modes at long periods.

Our approach is to carry out a rotated principal component analysis of the combined variability. The basic analysis uses the five variables as discussed in the introduction. However, the analysis has been repeated with one (SST) and three variables (SST and winds). Results for the three-variable case were qualitatively similar to those presented here.

Different variables should be normalized before carrying out a combined analysis. A common approach is to normalize each variable by its local standard deviation, thus making different variable types comparable in size, as well as removing the effects of differing spatial distributions of variability. Here we take the alternative approach of Nigam and Shen (1993) and normalize each variable by another measure of variability, the square root of the spatially integrated temporal variance. Additionally, before normalizing anomalies, an area weighting of the anomalies is done following Chung and Nigam (2000) in order to avoid overemphasizing the variability in the higher grid-density areas.

The eigenvalues and eigenvectors of the anomaly covariance matrix are obtained from the SVD analysis of the anomaly matrix. The eigenvectors are then rotated. Rotation relaxes the constraint of orthogonality of the spatial patterns but preserves this constraint for the principal component time series. By relaxing the spatial orthogonality constraint the spatial patterns of the rotated eigenvectors should be more directly related to the natural patterns of variability in the physical system (Richman 1986). A number of algorithm choices are possible for rotation. Here we follow Houghton and Tourre (1992) and apply the varimax technique using the IMSL (1989) FROTA routine. We also follow the usual practice and limit the number of eigenvectors to rotate. In the results presented below we use the first 10 eigenvectors that individually captured 2% or more of the combined variance (together explaining 38%). Experiments with 8 and 12 eigenvectors show that the results are insensitive to this choice.

Correlations between time series were calculated using the Fisher Z transformation. Confidence at the 95% level is obtained in those coeficients taking into account serial correlation (Angell 1981; Reid et al. 1989).

3. Coupled variability in the tropical Atlantic

In order to focus our attention on that fraction of the atmospheric and oceanic thermal and momentum fields associated with coupled variability we begin with a combined rotated principal component analysis of the complete set of monthly anomalies of all calendar months in a domain extending from 20°S to 30°N. The variables we choose are heat content (hc), sea surface temperature (sst), zonal and meridional wind stress (taux, tauy), and diabatic heating (q) anomalies. The mode that explains the largest fraction of shared variance (5.8%) has a spatial pattern that is primarily associated with movements of the subtropical wind system (poleward of 20°N), which is not the subject of this paper. The next two Tropics-related modes are shown in Figs. 1 and 2 and both explain the same 4.9% of the shared variance. These modes are clearly of significance as in the rotated analysis of SSTs alone, the corresponding SST modes account for 17% and 18.4% of the SST variance.[1]

a. Atlantic Niño

The SST signature of the second mode is mainly confined to the eastern equatorial region. The structure of this Atlantic equatorial anomaly pattern is more closely confined to the eastern basin, but spanning a broader range of latitudes than suggested by the results of Zebiak (1993). However, it is quite consistent with the SST anomaly pattern obtained by compositing warm events during the past several decades (1963, 1966, 1968, 1973–74, 1981, 1984, 1987, 1988) and, in particular to the well-documented SST anomaly pattern in 1984 (Carton and Huang 1994). Warming of SST in the eastern basin is accompanied by an eastward shift of warm water, a relaxation of the equatorial trade winds in the central basin, and a southward shift of convection. This picture resembles El Niño so we will refer to this mode as the Atlantic Niño. A spectral analysis (not shown) of the principal component of this mode has interdecadal and interannual (2.25 yr) peaks.

To determine the corresponding wind divergence associated with the pattern of diabatic heating in Fig. 1 we project the principal component time series onto the divergence at 850 and 200 mb. Examination of diabatic

[1] Explained variance amounts are comparatively smaller in *combined* variability analysis.

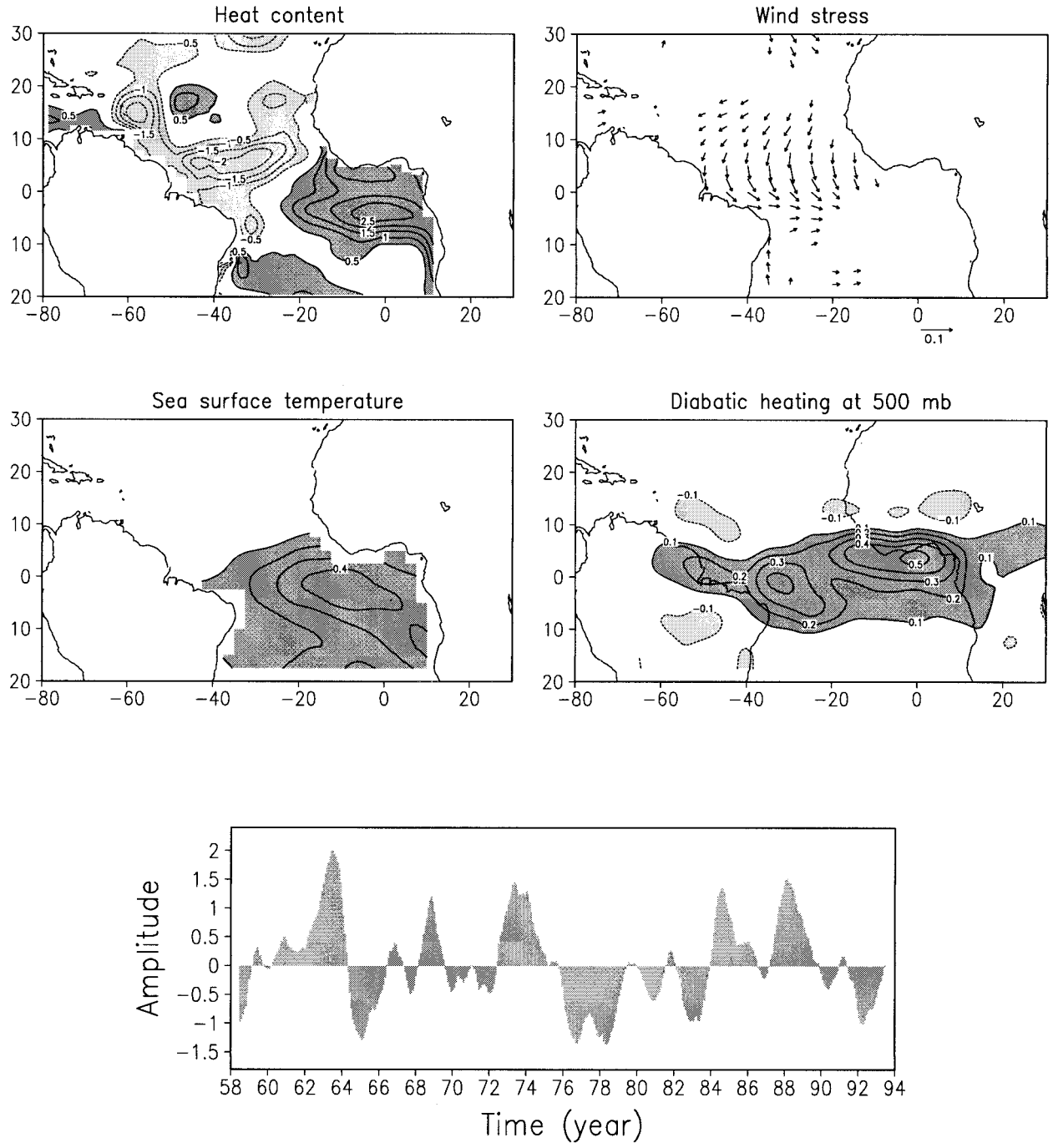

FIG. 1. Anomalies of the Atlantic Niño mode and its associated principal component coefficient (PCC) from a 5-variable rotated combined analysis: hc′ ($10^8 \times$ J m^{-2}) (upper left), tau′ (dyn cm^{-2}) (upper right), sst′ (°C) (middle left), q′ (°C day^{-1}) at 500 mb (middle right), and PCC smoothed with a 12-month running mean (lower). Only wind stress anomalies larger than 0.02 dyn cm^{-2} are shown. Explained variance is 4.9%. Dark (light) shading denotes positive (negative) anomalies.

heating in Fig. 1 shows positive heating anomalies to the southeast and negative anomalies to the north of the climatological maximum in heating (e.g., Fig. 1.4 in Philander 1990), suggesting that the intertropical convergence zone (ITCZ) has been shifted southward by the warming of surface waters. The divergence field is shown in the left panels of Fig. 3. It is worth noting that while the 200-mb anomalies are structurally similar to midtropospheric heating, the 850-mb anomalies are not, particularly, in the western sector. This reflects a change in the vertical distribution of equatorial heating across the Atlantic basin [see upcoming Fig 4, (top)].

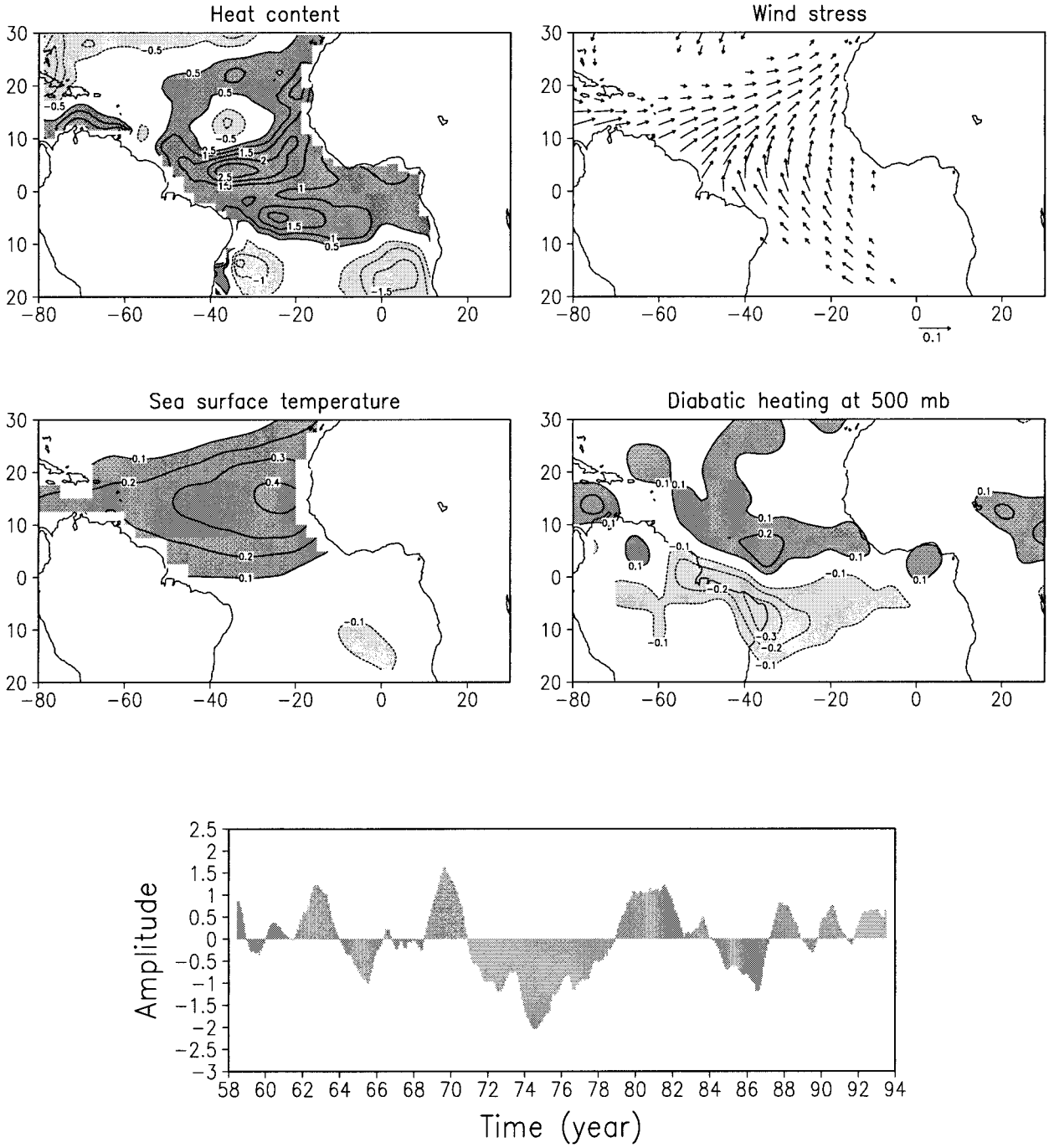

FIG. 2. Anomalies of the interhemispheric mode and its associated PCC from a 5-variable rotated combined analysis: hc′ ($10^8 \times$ J m^{-2}) (upper left), tau′ (dyn cm^{-2}) (upper right), sst′ (°C) (middle left), q′ (°C day^{-1}) at 500 mb (middle right), and PCC smoothed with a 12-month running mean (lower). Only wind stress anomalies larger than 0.02 dyn cm^{-2} are displayed. Explained variance is 4.9%. Shading as in Fig. 1.

The vertical structure of diabatic heating along the equator associated with the Atlantic Niño mode is shown in Fig. 4 (top). This vertical projection shows warming throughout the troposphere above 925 mb, extending far onto adjacent continents. The height of maximum heating shifts upward in the air column over the Amazon, while in the lowest 75 mb we find diabatic cooling. In order to determine the relative importance of individual terms in making up the full diabatic heating, we project the principal component time series on the individual heating terms from the NCEP reanalysis for the 1973–93 subperiod. The three-dimensional diabatic

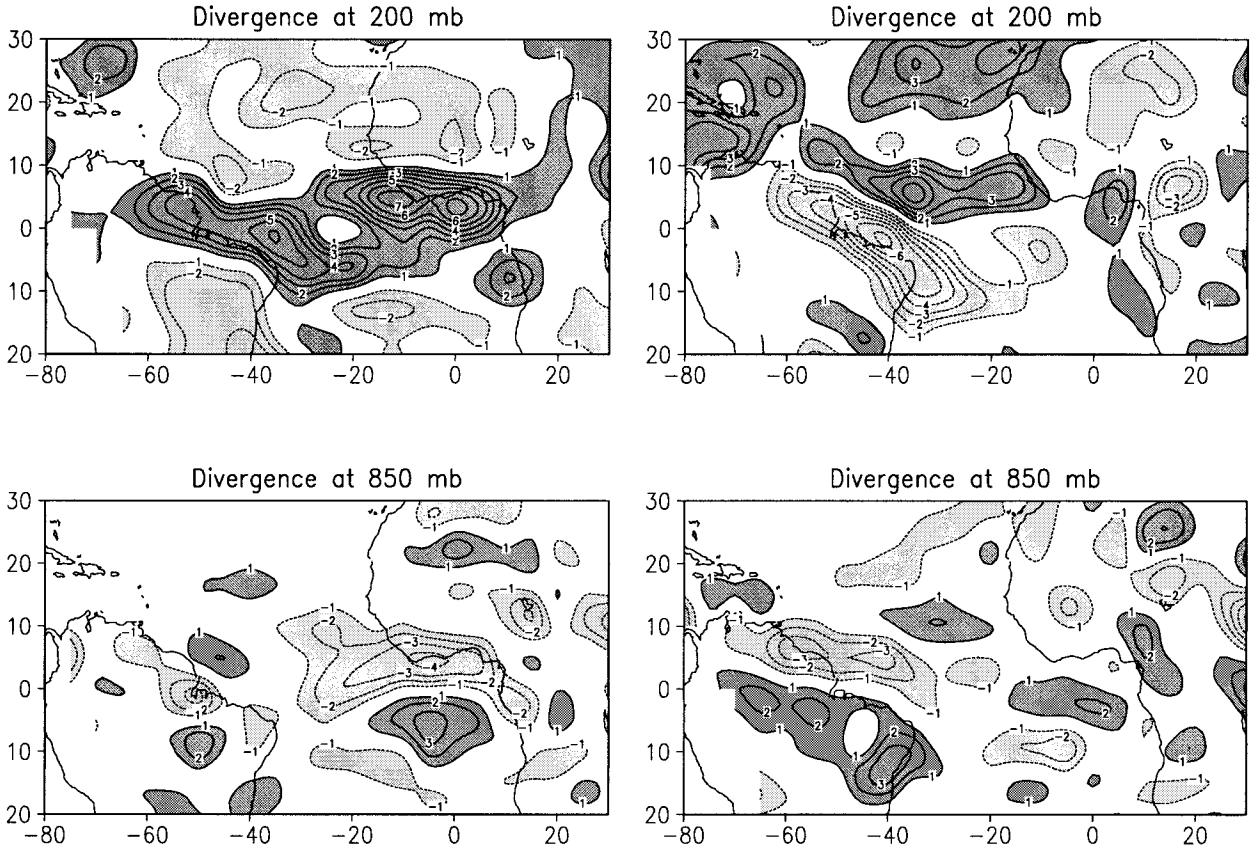

FIG. 3. Regression of divergence anomalies (10^{-7} s^{-1}) at 200 mb (top) and 850 mb (bottom) levels on the rotated PCC of the Atlantic Niño (left) and interhemispheric (right) modes. Dark (light) shading denotes divergence (convergence) anomalies.

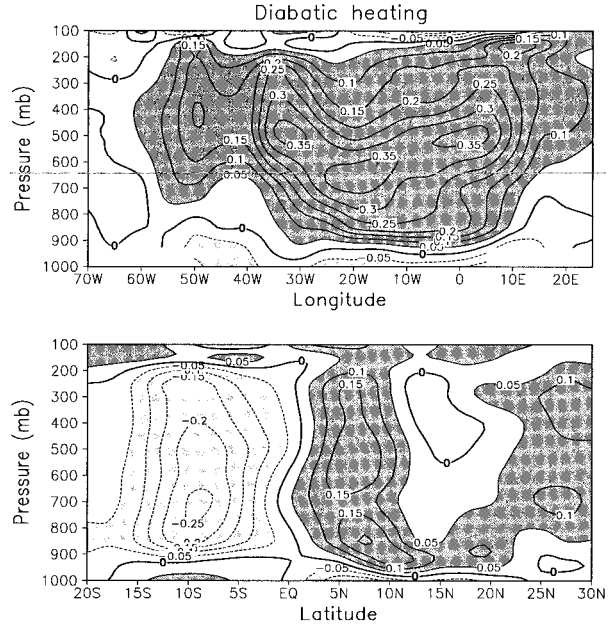

FIG. 4. Regression of averaged diabatic heating anomalies (°C day^{-1}) along 2.5°S–2.5°N and 26°–31°W on the rotated PCC of the Atlantic Niño (top) and interhemispheric (bottom) modes. Dark (light) shading denotes warming (cooling) anomalies.

heating components from the reanalysis data are generated during a 6-h model forecast. We find total diabatic heating is dominated by the release of latent heat induced in deep cloud formation [cf. Fig. 1 and Fig. 5 (top)]. Longwave radiation heating at 850 mb [Fig. 5 (bottom)] is positively correlated with the SST anomalies and deep convective heating. The longwave heating results from the trapping of longwave radiation beneath the tropical clouds. A similar distribution of heating occurs during ENSO variability, with longwave heating anomalies occurring as in the ''shadow'' of the deep convective heating anomalies (Nigam et al. 2000). At lower levels the cooling effect of evaporating rain becomes an important factor and causes the change of sign of diabatic heating in the lowest 75 mb observed in Fig. 4. We have repeated the examination using residually calculated diabatic heating from the shorter ECMWF reanalysis. The heating results resemble those displayed in Fig. 5 except that the values are higher on continental areas.

Regression of anomalies of precipitation (from the dataset of Xie and Arkin 1997) during the 1979–93 subperiod and anomalies of wind at 200 mb on the Atlantic Niño mode principal component time series show enhanced precipitation along the equatorial At-

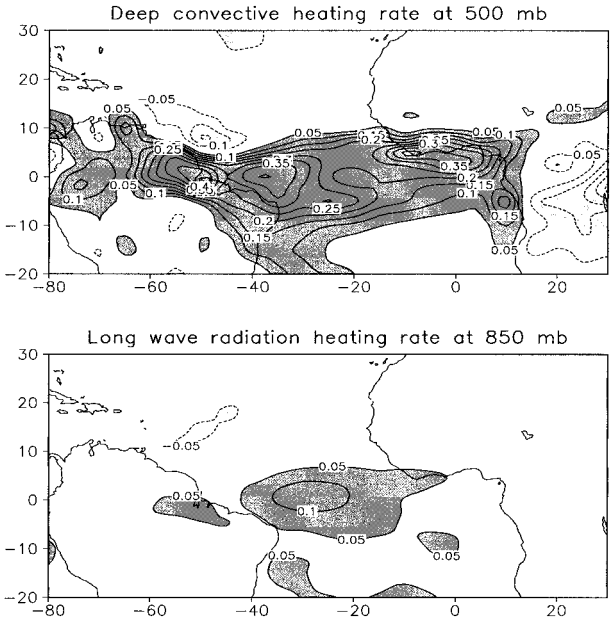

FIG. 5. Regression of anomalies of deep convective heating rate (°C day^{-1}) at 500 mb (top) and longwave radiation heating rate (°C day^{-1}) at 850 mb (bottom) on the rotated PCC of the Atlantic Niño mode during the 1973–93 subperiod. Shading as in Fig. 4.

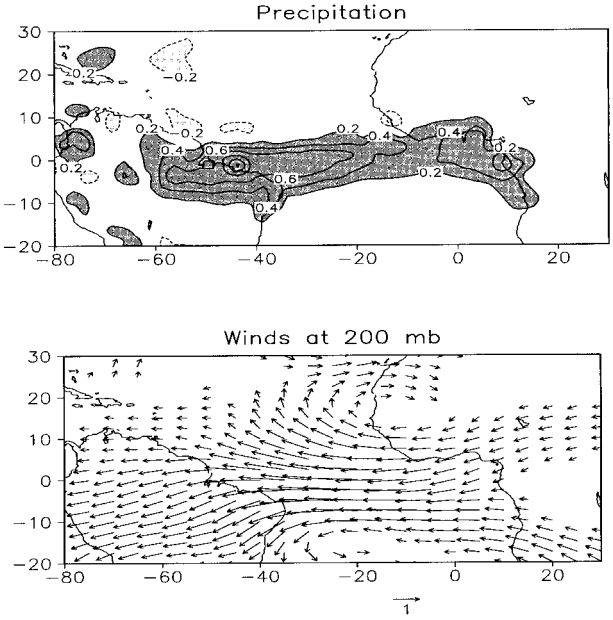

FIG. 6. Regression of anomalies of Xie and Arkin precipitation (mm day^{-1}) during the 1979–93 subperiod (top) and wind (m s^{-1}) at 200 mb (bottom) on the rotated PCC of the Atlantic Niño mode. Only wind amonalies larger than 0.3 m s^{-1} are displayed. Dark (light) shading denotes anomalous wet (dry) conditions.

lantic [Fig. 6 (top)] consistent with the deep convective heating anomalies displayed in Fig. 5. Precipitation over northeastern Brazil (averaged between 11°–1°S and 46°–36°W from Xie and Arkin 1997) during June–July–August has a correlation of 0.62 with this mode at 2-month lag. The associated upper-level wind anomalies at 200 mb [Fig. 6 (bottom)] show weakened westerlies and anticyclonic circulation resembling those of El Niño in the Pacific. The strengthened easterlies extend back to the eastern Pacific.

Finally, we consider the oceanic expression of the Atlantic Niño. The covarying temperature with depth and longitude (averaged 2.25°S–2.25°N) is shown in [Fig. 7 (top)], where the mean position of the thermocline is indicated by the depth of the 20°C isotherm. The thermocline is slightly deeper (8.5 m) than the values assumed by Zebiak (1993). Positive SSTs are associated with a deepening thermocline of approximately 4 m in the eastern basin and a shallowing thermocline of around 2 m in the west, as expected from the weakened trade winds. This profile in SST anomalies gives the observed structure in heat content depicted in Fig. 1. The similarity with the subsurface structure of El Niño is striking.

b. Interhemispheric mode

The third mode has a pattern in SST that is primarily evident in the Northern Hemisphere with maximum SST gradient near the thermal equator (Fig. 2). Because of this asymmetry, we refer to it as the interhemispheric

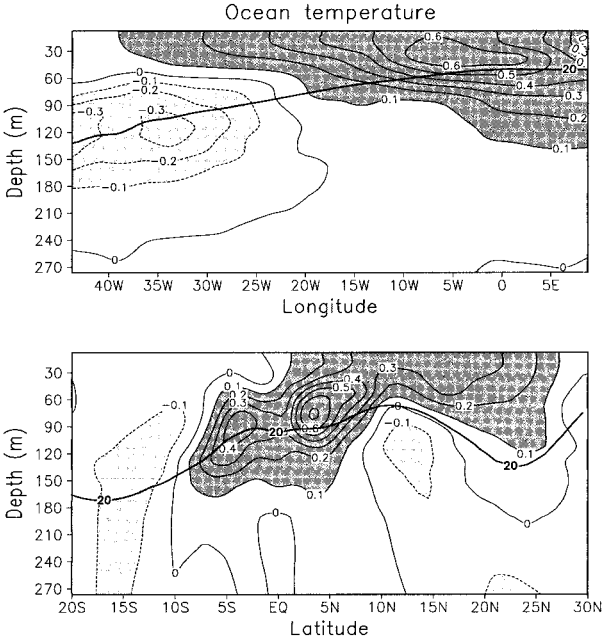

FIG. 7. Regression of averaged anomalies of ocean temperature (°C) along 2.5°S–2.5°N and 26°–31°W on the rotated PCC of the Atlantic Niño (top) and interhemispheric (bottom) modes. Bold line shows the mean position of the 20°C isotherm indicating the depth of the thermocline in the Tropics. Dark (light) shading denotes anomalous warm (cold) conditions.

mode, although it resembles the northern portion of the dipole mode of Hastenrath and Greischar (1993), Curtis and Hastenrath (1995), and Chang et al. (1997). Spectral analysis of the associated time series principal component of the interhemispheric mode (not shown) has a peak at 12 yr, consistent with some previous studies of the dipole mode (Moura and Shukla 1981; Servain 1991; Mehta and Delworth 1995).

In our interpretation, the wind field associated with the interhemispheric mode responds to the distribution of anomalous SST. A positive Northern Hemisphere SST anomaly produces a northward cross-equatorial wind stress anomaly and counterclockwise circulation in the warmer subtropics. The northern counterclockwise wind anomaly acts to weaken the background northeast trade winds, while the southern wind anomaly strengthens the background southeast trade winds. Changes in heat content are also evident. This mode results in anomalous downwelling of surface water in the warm hemisphere and along the equator consistent with the Ekman pumping effects. Interestingly, this pattern is interrupted by a negative anomaly at 12°N. Examination of Fig. 7 (bottom) shows that this negative anomaly is associated with anomalous uplifting of the thermocline. Less pervasive anomalous upwelling occurs in the cool hemisphere.

The interhemispheric mode is accompanied by a dipole pattern in diabatic heating. Positive anomalies occur over warm SST in the Northern Hemisphere, while negative anomalies occur over northeastern (Nordeste) Brazil and the southern tropical ocean.

The zone of negative diabatic heating anomaly over Nordeste, Brazil, is associated with divergence at 850 mb and convergence at 200 mb (Fig. 3, right-hand panels). Intensification of this pattern has been identified by Rao et al. (1995) as a possible cause of the drought in 1993. In fact, because the rainy season in Nordeste is during spring, the interhemispheric mode has a larger impact on its precipitation than the Atlantic Niño mode. Indeed, we can compare the years of observed droughts (at least a half of their standard deviation below average in 1958, 1966, 1979, 1980, 1983, 1990, and 1993) and floods [at least a half of their standard deviation above average in 1965, 1967, 1968, 1974, 1975, 1984, 1985, 1986, 1989, Hastenrath and Greischar (1993)] in the Nordeste region of Brazil (Rao et al. 1995) with the third mode principal component time series. The correlation of Nordeste rainfall (averaged between 11°–1°S and 46°–36°W) with the interhemispheric mode is −0.40 when all months are used and −0.70 when restricted to the rainy season (March–May). Warming in the northern tropical Atlantic Ocean can also set up favorable conditions for precipitation in the Caribbean (Taylor 1999).

The vertical structure of diabatic heating associated with the interhemispheric mode is presented in Fig. 4 (bottom). We find anomalous heating from 925 to 100 mb over anomalously warm SSTs north of the equator.

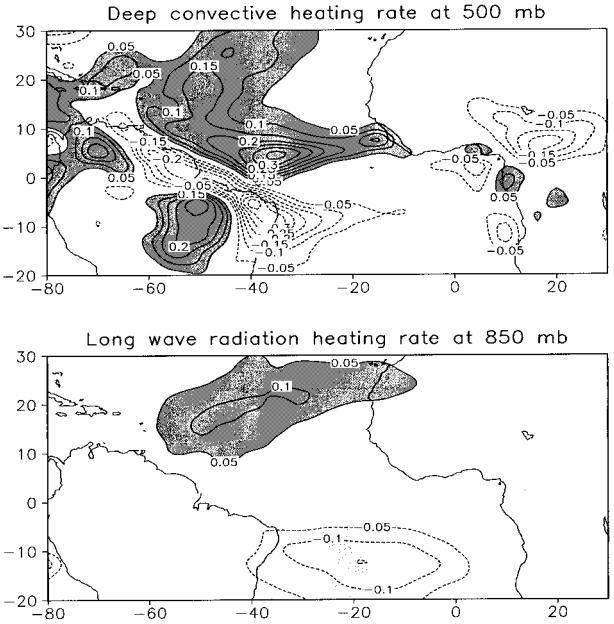

FIG. 8. Regression of anomalies of deep convective heating rate (°C day^{-1}) at 500 mb (top) and longwave radiation heating rate (°C day^{-1}) at 850 mb (bottom) on the rotated PCC of the interhemispheric mode during the 1973–93 subperiod. Shading as in Fig. 4.

South of the equator a region of anomalous cooling is associated with the northward shift of the ITCZ. Both north and south the sign of diabatic heating in the lowest 75 mb is of opposite sign to heating higher in the atmosphere, as was seen earlier with the Atlantic Niño mode. As in the case of that mode, the interhemispheric mode is dominated by deep convection (Fig. 8). The deep convective clouds in turn are responsible for anomalous precipitation [Fig. 9 (top)] over warm waters to the north. At 200-mb convection causes an intensification of the subtropical jets [Fig. 9 (bottom)] as noted by Marengo and Hastenrath (1993). The opposite phase of the mode leads to a weakening of the subtropical jets and an increase in precipitation over Nordeste, Brazil.

Finally, we explore the oceanic projection of the interhemispheric mode [Fig. 7 (bottom)]. It is evident that northern SST anomalies penetrate to thermocline depths and extend southward across the equator. The associated thermocline depth anomalies are around 3 m. These anomalies and their associated negative anomalies of heat content in the northern subtropic at 12°N [Fig. 2 (upper left panel)], appear to be the result of a positive anomaly of wind-induced Ekman pumping on the northern side of the North Equatorial Countercurrent. This result suggests an active role of enhanced surface currents transporting warm waters meridionally. This effect is absent in the modeling study by Xie and Tanimoto (1998), who consider a mixed layer of constant depth.

4. Seasonal dependence

The results presented in section 3 suggest that both the Atlantic Niño and interhemispheric modes are sub-

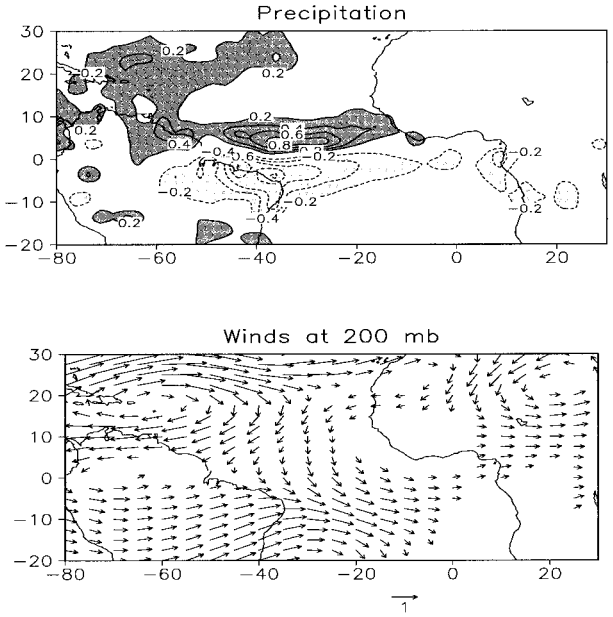

FIG. 9. Regression of anomalies of Xie and Arkin precipitation (mm day^{-1}) during the 1979–93 subperiod (top) and wind (m s^{-1}) at 200 mb (bottom) on the rotated PCC of the interhemispheric mode. Only wind anomalies larger than 0.3 m s^{-1} are displayed. Shading as in Fig. 6.

ject to strong seasonal influences. In the case of the Atlantic Niño mode the maximum SST anomalies occur in boreal summer when cold 23°C water normally appears on the equator. In the case of the interhemispheric mode the meridional gradient of SST undergoes seasonal changes, reaching a maximum on and north of the equator in boreal spring. In this section we explore the dependence on season by repeating the analysis limiting the data to boreal summer (June–July–August) and spring (March–April–May).

In summer the Atlantic Niño mode is now the largest, explaining 7.5% of the total variance. The trade wind anomalies become more symmetric about the equator, while the negative (positive) heating anomalies north (south) of the climatological position of the ITCZ are more evident than those of the annual analysis of Fig. 1. In addition to shifting, the convergence strengths over the warm water reinforcing the impression of a southward shift of the ITCZ.

Our rotated principal component analysis assumes that the response to positive and negative SST anomalies is similar. We examine this assumption by compositing fields separately for extreme positive and negative phases of the Atlantic Niño mode. The composites do reveal asymmetries. While anomalously high equatorial SSTs are associated with anomalously high heat content and a depressed thermocline, anomalously low SSTs are not generally associated with anomalously low heat content. The composities also reveal that the relaxation of trade winds during warm events is most pronounced in early summer (June).

When the analysis is limited to spring the interhemispheric mode is largest, nearly doubling its share of explained variance to 9.1%. This new first mode shows a stronger response in SST in the Southern Hemisphere than when all months were used for the analysis. But as before, SST anomalies are associated with thermocline anomalies of the same sign. The heating fields from the spring analysis differ from those of the annual analysis of Fig. 2 mainly in the increase in continental heating. Compositing extreme positive and negative events of the interhemispheric mode gives reassuringly similar results. In this case, composites show that relaxation of the northeasterly trade winds is strongest during early spring (March) of the northern warm events and that a build up of ocean heat content starts just past of the Caribbean region, spreading to the east in the following months.

5. Nonlocal influences

In this section we consider the role that other regions, specifically the North Atlantic and tropical Pacific, may play in generating and responding to the tropical Atlantic. Recent results summarized in the introduction have suggested a relationship between the interhemispheric mode and the NAO—defined here as the surface air pressure difference between the Azores and Iceland.

One way to explore the tropical–North Atlantic connection is to expand the domain of our analysis to include both regions (here we expand to 60°N). This expanded analysis shows the same three modes previously obtained. The first mode bears a good correlation (-0.54) with the NAO index, while the interhemispheric mode has a maximum -0.11 correlation when lagging the NAO index by 3 months and the Atlantic Niño mode is uncorrelated. Efforts to improve the correlation by lows-pass filtering the data did not improve the results. Thus, it seems that the interhemispheric mode and the NAO are two separate modes of variability. In order to investigate this further we project the normalized NAO index and interhemispheric mode PC time series, for the period 1958–93, on anomalies of sea surface temperature. Comparison between the two shows 1) that the NAO does not have a significant projection at tropical latitudes [Fig. 10 (top)] and 2) that the interhemispheric mode extends to midlatitudes [Fig. 10 (bottom)]. Thus, our results support the idea that tropical variability (from the interhemispheric mode) may affect the North Atlantic variability, possibly through a weakening of the subtropical anticyclone (e.g., Rajagopalan et al. 1998), and not in the other way around (as suggested by Xie and Tanimoto 1998).

The relationship between the interhemispheric mode and Pacific variability also needs to be considered. We begin by examining the correlation between the interhemispheric mode principal component time series and the Southern Oscillation index, and Niño-3 (5°S–5°N, 150°–90°W), and Niño-4 (5°S–5°N, 160°E–150°W) SST

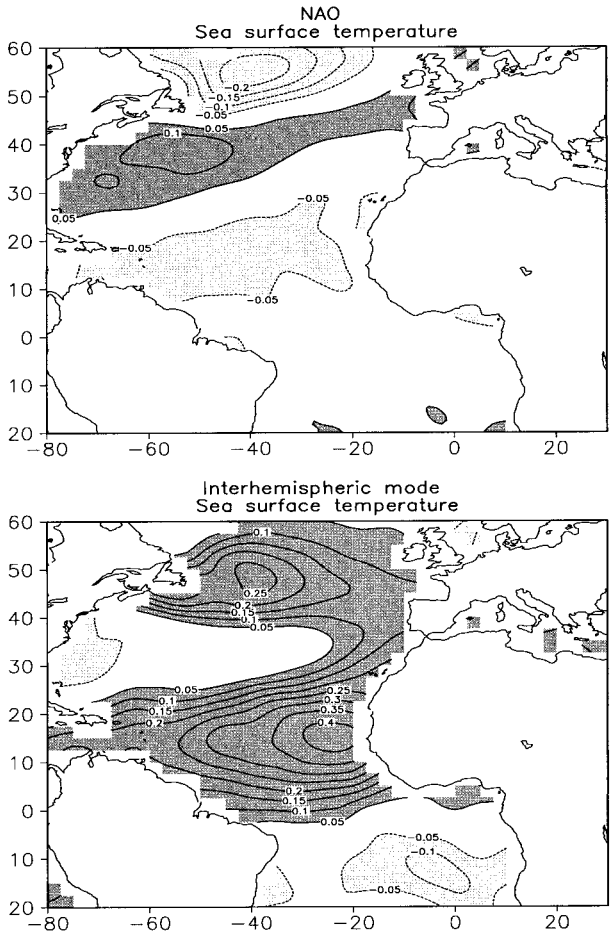

FIG. 10. Regression of anomalies of sea surface temperature (°C) on the normalized NAO index (top) and interhemispheric mode PCC time series (bottom). Dark (light) shading denotes anomalous warm (cold) conditions.

indices. Of these, the correlation with Niño-4 was slightly larger and so we focus on this index. When we regress the Niño-4 index on all five tropical Atlantic variables spatial patterns emerge (Fig. 11) that resemble all panels of the interhemispheric mode of Fig. 2. This similarity of spatial pattern would seem to suggest that the interhemispheric mode is driven by Pacific variability. Indeed, the correlation between the Niño-4 index and the interhemispheric mode time series reaches 0.44 when the former leads the latter by four to five months (in agreement with results of Lanzante 1996 and Enfield and Mayer 1997, who found a 0.5 correlation at 4–5-month lag). When the comparison is made only between Niño-4 during November–December–January and the interhemispheric mode principal component during the following March–April–May the correlation increases to 0.62 (suggesting that roughly 30% of the variance of the interhemispheric mode during this season is being forced by events in the Pacific, close to the 25% that Enfield and Mayer attribute to the same effect). We would like to be able to remove this forced signal from our analysis in order to examine the variability not associated with the Pacific. We do this first by removing the variability from our tropical Atlantic data that is covarying with the Niño-4 time series. We then repeat the analysis of Figs. 1 and 2 on this filtered data. The resulting filtered analysis still shows the interhemispheric mode except for a reduction in the magnitude of the anomalies and their associated gradients. This give us reassurance that the interhemispheric mode derived from the unfiltered data mainly represents variability intrinsic to the Atlantic sector. El Niño events affect the interhemispheric mode somewhat at interannual scales.

We also examine the relationship between the Atlantic Niño and Niño-4. Here we find a maximum correlation of -0.33 at 12-month lead (and -0.26 correlation with Niño-3 index at 6-month lead), consistent with the results by Servain (1991). From these results is evident that the connection between ENSO and the tropical Atlantic is strongest in the north and that equatorial warming events are not highly correlated with events in the tropical Pacific.

6. Summary and discussion

This study represents a search for covarying air/sea modes of variability in the tropical Atlantic sector in retrospective analyses of the atmosphere and ocean spanning the years 1958–93. We use a rotated principal component analysis to search for coherent variations in four key parameters, sea surface temperature, winds, atmospheric diabatic heating, and ocean heat content. Our analysis focuses on two covarying modes we refer to as the Atlantic Niño and the interhemispheric mode. Aspects of these modes have been previously described, but other features are new. The expanded view of these modes arise as a consequence of the combined analysis we use. Here we focus on the relationships among atmospheric and oceanic variables and relationships to variability in other basins. The Atlantic Niño has a principal component that varies at interannual as well as longer interdecadal periods, although the latter timescale is not well resolved by our analysis. The mode is strongly linked to the seasonal cycle, with maximum amplitude in northern summer, the season when a cold tongue of water normally appears in the east along the equator.

The positive phase of this mode thus results in the absence of a cold tongue. The trade winds along the equator weaken west of 20°W, while warm thermocline water is shifted eastward. These westerly wind anomalies persist up to a height of 700 mb and are associated with enhanced convergence of winds below this level. Winds at 200 mb display anticyclonic circulations in both hemispheres. Convection is increased south of the normal position of the ITCZ while somewhat reduced farther north. Increased diabatic heating occurs throughout the troposphere over the anomalously warm water. The direct connection between ENSO and the Atlantic

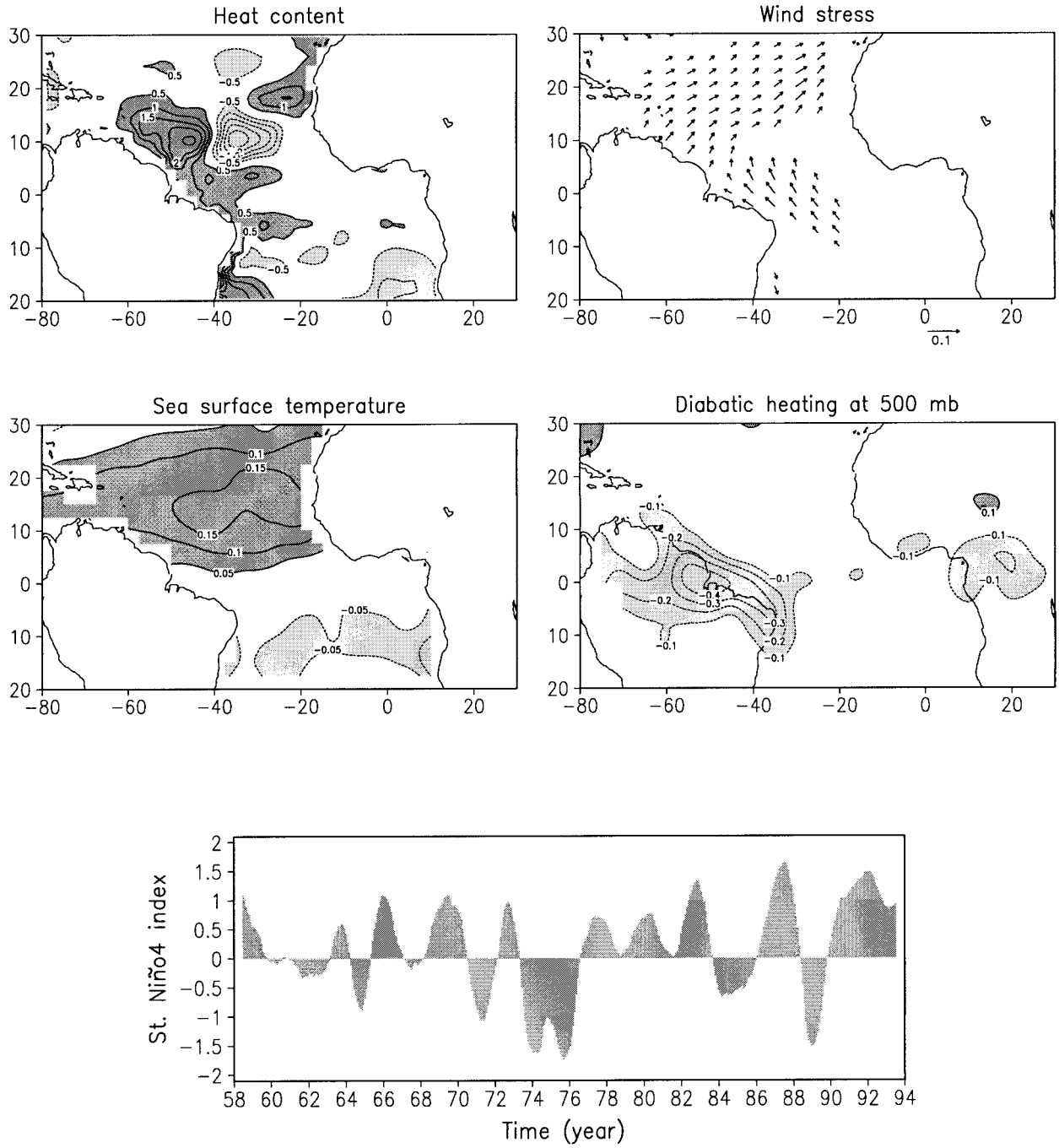

FIG. 11. Regression of anomalies of hc ($10^8 \times$ J m^{-2}) (upper left), tau (dyn cm^{-2}) (upper right), sst (°C) (middle left), and q (°C day^{-1}) at 500 mb (middle right), on the normalized Niño-4 index. Normalized Niño-4 index time series is smoothed with a 12-month running mean (lower panel). Only wind stress anomalies larger than 0.02 dyn cm^{-2} are displayed. Shading as in Fig. 1.

Niño seems to be weak, although it can exist indirectly as suggested by Carton and Huang (1994).

The second mode we identify is one we refer to as the interhemispheric mode. This mode has longer decadal timescales (12 yr). It is linked to the seasonal cycle with strongest variations in northern spring. Its corresponding pattern of anomalous SST has an interhemispheric gradient with larger fluctuations of the SST in the Northern Hemisphere than the Southern Hemisphere. Its winds indicate a response to an SST gradient consisting of strong cross-equatorial flow into the warm hemisphere and eastward curvature. Positive diabatic heating occurs in the warm hemisphere throughout the troposphere from 975 to 200 mb with negative anom-

alies in the lowest 75 mb over warm water. The cause of this low-level diabatic cooling seems to be evaporation of raindrops (as occurs in areas of intense precipitation as pointed out by Hastenrath 1991). Winds at 200 mb indicate a strengthening of the subtropical jets in connection with enhanced precipitation to the north and west of the equatorial Atlantic. For both the Atlantic Niño and interhemispheric modes deep convection is the most important term in the balance of anomalous diabatic heating.

The relation between the interhemispheric mode and the climate of other ocean basins appears more complicated than for the Atlantic Niño. By expanding the domain of analysis we find that a positive phase of the interhemispheric mode covaries with warm SST and weakened westerlies to the southeast of Newfoundland around 45°N. Yet, the NAO, a widely discussed index of the movement of North Atlantic storm tracks, is not well correlated with the interhemispheric mode principal component time series. Regressions of atmospheric and oceanic variables on the normalized NAO index and the interhemispheric mode principal component time series lead us to conclude that they are two separate modes of variablity in the Atlantic. However, there is some possibility that the interhemispheric mode may affect North Atlantic variability and eventually the NAO as suggested by Rajagopalan et al. (1998). These results are not consistent with the suggestion of Xie and Tanimoto (1998) that midlatitude variability drives tropical variability or of Robertson et al. (1998) who suggest an influence of southern Tropics on NAO.

On the other hand, variability in the tropical Pacific Ocean does bear a significant relationship to the interhemispheric mode. When indicators of Pacific variability such as the Niño-4 index are regressed on tropical Atlantic variability, patterns do emerge that resemble the interhemispheric mode. An examination of the lag correlation between the two reveals a maximum 0.44 correlation when the Pacific leads the Atlantic by 4–5 months. However, when this covarying signal is removed from tropical Atlantic variables and the analysis is repeated the spatial patterns and principal component time series of the interhemispheric mode are still there except for a weakening of the gradients. This result is consistent with the observation that the timescales of variation of the Niño-4 SST and the interhemispheric mode are quite different. Thus we are left with the complicated result that spatial patterns resembling the interhemispheric mode may be forced by Pacific variability, but that much of the energy in the interhemispheric mode cannot be explained simply in terms of remote influence and probably results from interactions within the tropical Atlantic sector itself. Exploration of these mechanisms may need to await the development of realistic coupled models.

Acknowledgments. The authors are grateful to Dr. C. Chung for his assistance with the principal component analysis, and to Dr. Eric DeWeaver for diagnosing the diabatic heating from the NCEP reanalysis. AR-B was supported by a scholarship from the National University of Mexico. JAC was supported by the National Science Foundation (OCE9530220) and NASA (NASA960912). SN was supported by NOAA PACS Grant NA76GP0479, and NSF Grant ATM9422507.

REFERENCES

Angell, J. K., 1981: Comparison of variations in atmospheric quantities with sea surface temperature variations in the equatorial eastern Pacific. *Mon. Wea. Rev.*, **109,** 230–243.

Carton, J. A., and B. Huang, 1994: Warm events in the tropical Atlantic. *J. Phys. Oceanogr.*, **24,** 888–903.

——, X. Cao, B. S. Giese, and A. M. da Silva, 1996: Decadal and interannual SST variability in the tropical Atlantic Ocean. *J. Phys. Oceanogr.*, **26,** 1165–1175.

——, G. Chepurin, X. Cao, and B. Giese, 2000a: A Simple Ocean Data Assimilation analysis of the global upper ocean 1950–95. Part I: Methodology. *J. Phys. Oceanogr.*, **30,** 294–309.

——, ——, and ——, 2000b: A Simple Ocean Data Assimilation analysis of the global upper ocean 1950–95. Part II: Results. *J. Phys. Oceanogr.*, **30,** 311–326.

Chang, P., L. Ji, and H. Li, 1997: A decadal climate variation in the tropical Atlantic Ocean from thermodynamic air–sea interactions. *Nature,* **385,** 516–518.

Chepurin, G., and J. A. Carton, 1999: Comparison of retrospective analyses of the global ocean heat content. *Dyn. Atmos. Oceans,* **29,** 119–145.

Chung, C., and S. Nigam, 2000: Weighting of geophysical data in principal component analysis. *J. Geophys. Res.*, in press.

Clarke, A. J., and A. Lebedev, 1997: Interannual and decadal changes in equatorial wind stress in the Atlantic, Indian, and Pacific Oceans and the eastern ocean coastal response. *J. Climate,* **10,** 1772–1729.

Curtis, S., and S. Hastenrath, 1995: Forcing of anomalous sea surface temperature evolution in the tropical Atlantic during Pacific warm events. *J. Geophys. Res.*, **100,** 15 835–15 847.

da Silva, A. M., A. C. Young, and S. Levitus, 1994: *Algorithms and Procedures.* Vol. 1, *Atlas of Surface Marine Data 1994.* National Oceanic and Atmospheric Administration, 83 pp.

Delworth, T. L., and V. M. Mehta, 1998: Simulated interannual to decadal variability in the tropical and subtropical North Atlantic. *Geophys. Res. Lett.*, **25,** 2825–2828.

Enfield, D. B., and D. A. Mayer, 1997: Tropical Atlantic SST variability and its relation to El Niño–Southern Oscillation. *J. Geophys. Res.*, **102,** 929–945.

Hastenrath, S., 1991: *Climate Dynamics of the Tropics,* Vol. 8. Kluger Academic Publishers, 488 pp.

——, and L. Greischar, 1993: Circulation mechanisms related to northeast Brazil rainfall anomalies. *J. Geophys. Res.*, **98,** 5093–5102.

Hisard, P., 1980: The ''El Niño'' response of the eastern tropical Atlantic. *Oceanol. Acta*, **3,** 69–78.

Houghton, R. W., and Y. M. Tourre, 1992: Characteristics of low-frequency sea surface temperature fluctuations in the tropical Atlantic. *J. Climate,* **5,** 765–771.

IMSL, 1989: International Mathematical and Statistical Library Version 1.1. IMSL Publication.

Lanzante, J. R., 1996: Lag relationships involving tropical sea surface temperatures. *J. Climate,* **9,** 2568–2578.

Marengo, J. A., and S. Hastenrath, 1993: Case studies of extreme climatic events in the Amazon basin. *J. Climate,* **6,** 617–627.

Mehta, V. M., 1998: Variability of the tropical ocean surface temperatures at decadal–multidecadal timescales. Part I: The Atlantic ocean. *J. Climate,* **11,** 2351–2375.

——, and T. L. Delworth, 1995: Decadal variability of the tropical

Atlantic ocean surface temperature in shipboard measurements and in a global ocean–atmosphere model. *J. Climate,* **8,** 172–190.

Merle, J., 1980: Variabilite thermique et interannuelle de l'Ocean Atlantique equatorial Est. L'hypothese d'un ''El Niño'' Atlantique. *Oceanol. Acta,* **3,** 209–220.

Moura, A. D., and J. Shukla, 1981: On the dynamics of the droughts in northeast Brazil: Observations, theory and numerical experiments with a general circulation model. *J. Atmos. Sci.,* **38,** 2653–2675.

Nigam, S., 1994: On the dynamical basis for the Asian summer monsoon rainfall–El Niño relationship. *J. Climate,* **7,** 1750–1771.

——, and H.-S. Shen, 1993: Structure of oceanic and atmospheric low-frequency variability over the tropical Pacific and Indian Oceans. Part I: COADS observations. *J. Climate,* **6,** 657–676.

——, C. Chung, and E. DeWeaver, 2000: ENSO diabatic heating in ECMWF and NCEP reanalyses, and NCAR CCM3 simulation. *J. Climate,* **13,** 3152–3171.

Nobre, P., and J. Shukla, 1996: Variations of sea surface temperature, wind stress, and rainfall over the tropical Atlantic and South America. *J. Climate,* **9,** 2464–2479.

Philander, S. G. H., 1990: *El Niño, La Niña and the Southern Oscillation.* International Geophysics Series, Vol. 46, Academic Press, 293 pp.

Rajagopalan, B., Y. Kushnir, and Y. M. Tourre, 1998: Observed decadal midlatitude and tropical Atlantic climate variability. *Geophys. Res. Lett.,* **25,** 3967–3970.

Rao, V. B., K. Hada, and D. L. Herdies, 1995: On the severe drought of 1993 in northeast Brazil. *Int. J. Climatol.,* **15,** 697–704.

Reid, G. C., K. S. Gage, and J. R. McAfee, 1989: The thermal response of the tropical atmosphere to variations in equatorial Pacific sea surface temperatures. *J. Geophys. Res.,* **94,** 14 705–14 716.

Richman, M. B., 1986: Rotation of principal components. *Int. J. Climatol.,* **6,** 293–335.

Robertson, A. W., C. R. Mechoso, and Y.-J. Kim, 2000: The influence of Atlantic sea surface temperature anomalies on the North Atlantic Oscillation. *J. Climate,* **13,** 122–138.

Servain, J., 1991: Simple climatic indices for the tropical Atlantic Ocean and some applications. *J. Geophys. Res.,* **96,** 15 137–15 146.

Tanimoto, Y., and S.-P. Xie, 1999: Ocean–atmosphere variability over the Pan–Atlantic basin. *J. Meteor. Soc. Japan,* **77,** 31–46.

Taylor, M. A., 1999: October in May: The effect of warm tropical Atlantic SST on early season Caribbean rainfall. Ph.D. thesis, University of Maryland, 213 pp.

Tourre, Y., B. Rajagopalan, and Y. Kushnir, 1999: Dominant patterns of climate variability in the Atlantic Ocean during the last 136 years. *J. Climate,* **12,** 2285–2299.

Weare, B. C., 1977: Empirical orthogonal analysis of Atlantic Ocean surface temperatures. *Quart. J. Roy. Meteor. Soc.,* **103,** 467–478.

Xie, P., and P. A. Arkin, 1997: Global Precipitation: A 17-year monthly analysis based on gauge observations, satellite estimates, and numerical model outputs. *Bull. Amer. Meteor. Soc.,* **78,** 2539–2558.

Xie, S.-P., and Y. Tanimoto, 1998: A Pan–Atlantic decadal climate oscillation. *Geophys. Res. Lett.,* **25,** 2185–2188.

Zebiak, S. E., 1993: Air–sea interaction in the equatorial Atlantic region. *J. Climate,* **6,** 1567–1586.